2013

Extending Airborne Electromagnetic Surveys for Regional Active Layer and Permafrost Mapping with Remote Sensing and Ancillary Data, Yukon Flats Ecoregion, Central Alaska

Neal J. Pastick
Stinger Ghaffarian Technologies, Inc., njpastick@usgs.gov

M. Torre Jorgenson
Alaska Ecoscience

Bruce K. Wylie
USGS EROS, Sioux Falls, SD, wylie@usgs.gov

Burke J. Minsley
USGS, Crustal Geophysics and Geochemistry Science Center, Denver, CO, bminsley@usgs.gov

Lei Ji
Arctic Slope Regional Corporation Research and Technology Solutions, Research and Technology Solutions

See last page for additional authors

PERMAFROST AND PERIGLACIAL PROCESSES
Permafrost and Periglac. Process. **24**: 184–199 (2013)
Published online 29 April 2013 in Wiley Online Library
(wileyonlinelibrary.com) DOI: 10.1002/ppp.1775

Extending Airborne Electromagnetic Surveys for Regional Active Layer and Permafrost Mapping with Remote Sensing and Ancillary Data, Yukon Flats Ecoregion, Central Alaska

Neal J. Pastick,[1]* *M. Torre Jorgenson,*[2] *Bruce K. Wylie,*[3] *Burke J. Minsley,*[4] *Lei Ji,*[5] *Michelle A. Walvoord,*[6] *Bruce D. Smith,*[4] *Jared D. Abraham*[4] *and Joshua R. Rose*[7]

[1] Stinger Ghaffarian Technologies, Inc., Contractor to the US Geological Survey (USGS) Earth Resources Observation and Science (EROS) Center, Sioux Falls, SD, USA
[2] Alaska Ecoscience, Fairbanks, AK, USA
[3] USGS EROS, Sioux Falls, SD, USA
[4] USGS, Crustal Geophysics and Geochemistry Science Center, Denver, CO, USA
[5] Arctic Slope Regional Corporation Research and Technology Solutions, Research and Technology Solutions, Contractor to the USGS EROS Center, Sioux Falls, SD, USA
[6] USGS, National Research Program, Denver, CO, USA
[7] Yukon Flats National Wildlife Refuge, Fairbanks, AK, USA

Machine-learning regression tree models were used to extrapolate airborne electromagnetic resistivity data collected along flight lines in the Yukon Flats Ecoregion, central Alaska, for regional mapping of permafrost. This method of extrapolation ($r = 0.86$) used subsurface resistivity, Landsat Thematic Mapper (TM) at-sensor reflectance, thermal, TM-derived spectral indices, digital elevation models and other relevant spatial data to estimate near-surface (0–2.6-m depth) resistivity at 30-m resolution. A piecewise regression model ($r = 0.82$) and a presence/absence decision tree classification (accuracy of 87%) were used to estimate active-layer thickness (ALT) (< 101 cm) and the probability of near-surface (up to 123-cm depth) permafrost occurrence from field data, modelled near-surface (0–2.6 m) resistivity, and other relevant remote sensing and map data. At site scale, the predicted ALTs were similar to those previously observed for different vegetation types. At the landscape scale, the predicted ALTs tended to be thinner on higher-elevation loess deposits than on low-lying alluvial and sand sheet deposits of the Yukon Flats. The ALT and permafrost maps provide a baseline for future permafrost monitoring, serve as inputs for modelling hydrological and carbon cycles at local to regional scales, and offer insight into the ALT response to fire and thaw processes. Published 2013. This article is a U.S. Government work and is in the public domain in the USA.

KEY WORDS: active-layer thickness; airborne electromagnetic; Alaska; cryosphere; permafrost; remote sensing

INTRODUCTION

Recent observations of increasing permafrost degradation (Jorgenson *et al*., 2001a, 2006) reinforce the need for accurately mapping the spatial extent of active-layer thickness (ALT) and permafrost in order to improve ecological monitoring and land management. In the past, only generalised maps have been available on regional scales, while site-scale maps have been limited to areas of intensive infrastructure development (Kreig, 1977). The regional maps are often associated with broad mapping units (e.g. discontinuous, continuous permafrost zones), and lack horizontal and vertical detail about permafrost extent and ALT (Anderson *et al*., 1973; Ferrians, 1965; Jorgenson *et al*., 2008; Hachem *et al*., 2009). Higher-resolution permafrost information is essential for monitoring change, land management, ecological modelling, and predicting future hydrologic, geomorphic and ecological impacts.

Mapping the spatial distribution of permafrost over large areas is challenging because of the need to associate surface characteristics with subsurface permafrost properties (Duguay *et al*., 2005; Panda *et al*., 2010, 2012). Traditional manual interpretation of aerial photographs and high-resolution satellite imagery has relied on the spatial extrapolation of permafrost from ground measurements and boreholes, based on changes in topography, surficial geology, hydrography, vegetation and conceptual models based on the field experience of the mapper

*Correspondence to: N. J. Pastick, Stinger Ghaffarian Technologies, Inc., Contractor to the USGS EROS Center, Sioux Falls, SD 57198, USA. E-mail: njpastick@usgs.gov

Received 26 April 2012
Revised 25 February 2013
Accepted 7 March 2013

(Kreig, 1977; Reger *et al*., 2012), while some progress has been made in automated pattern detection techniques (Roth *et al*., 2005). Such techniques for high-resolution mapping are limited to local scales, however, due to the high cost of data collection, time constraints and the difficulties of accessing remote areas.

For broader regions, automated image-processing techniques have been used to map permafrost, employing remotely sensed data (e.g. Landsat Thematic Mapper (TM), SPOT High Resolution Visible and topography) and spatial statistical techniques, including logistic discriminant functions (Morrissey *et al*., 1986; Panda *et al*., 2010, 2012), neural network classifiers (Peddle *et al*., 1991), classification and regression tree analyses, and basal temperature of snow (BTS) methods. The BTS method has proved useful (Lewkowicz and Ednie, 2004) for determining the probability of permafrost occurrence, but requires extensive field data collection in winter. The classification and regression tree analyses have also proved useful for mapping and modelling the probability of permafrost occurrence in mountainous regions (Kremer *et al*., 2011). These efforts, however, have been limited in spatial scale or use relatively few input variables, inhibiting the ability of models to represent complex biophysical relations across diverse environmental conditions.

Electromagnetic resistivity techniques have long been used to map subsurface characteristics (Joesting, 1941; Hoekstra *et al*., 1975), and recent advances in airborne electromagnetic (AEM) instrumentation and data processing have improved the effectiveness of the techniques for imaging permafrost and subsurface hydrogeological features (Kneisel *et al*., 2008; Siemon *et al*., 2009; Minsley *et al*., 2012). In Alaska, hundreds of AEM surveys have been conducted from 1999 to 2011 to investigate mineral resources and to aid permafrost mapping along the Alaska Highway road corridor (Burns *et al*., 2006), but rigorous data processing for permafrost mapping has been limited. The resistivity data are useful for differentiating frozen and unfrozen soils because frozen materials are more resistive than their unfrozen counterparts, although this relationship is complicated by the effects of material type and water content (Hoekstra *et al*., 1975; Daniels *et al*., 1976; Kawaski and Osterkamp, 1989). While AEM surveys typically are used to infer subsurface properties at intermediate depths (10–100 m) (Siemon *et al*., 2009), they are limited by the spatial extent of the linear survey flight lines. In this study, we used resistivity models derived from AEM data (Ball *et al*., 2011) and focused on results from the upper few metres, which serve as a proxy for the presence/absence of shallow permafrost.

The goal of this study was to map ALT and the presence or absence of near-surface permafrost at 30-m resolution throughout the Yukon Flats Ecoregion (YFE) of central Alaska. To achieve this goal, we: (1) compiled AEM and field active-layer measurements for model inputs; (2) developed maps of terrain characteristics of the YFE derived from satellite imagery and ancillary data related to topography, surficial geology, soil moisture, surface temperature, vegetation and spectral characteristics; (3) spatially modelled near-surface (0–2.6-m depth) resistivity (NSR) across the YFE at 30-m resolution using piecewise regression; and (4) spatially modelled ALT and near-surface permafrost from field data, predicted resistivity, and satellite and ancillary data using piecewise regression trees and decision tree classification.

STUDY AREA

The YFE is located approximately 160 km north of Fairbanks, Alaska, and encompasses an area of 33 400 km^2 (Nowacki *et al*., 2002). The YFE comprises relatively low-lying active and abandoned floodplains, surrounded by steeper hillslopes (Figure 1). The study area contains two main surficial deposits: (1) alluvial sediments in the low-lying and northern portion of the YFE; and (2) aeolian loess in the higher elevated southern and eastern portion of the YFE. Dominant forest vegetation types within the YFE (these data from the Fish and Wildlife Service are available at http://alaska.fws.gov/nwr/yukonflats/) are primarily black spruce (*Picea mariana*), paper birch (*Betula papyrifera*), quaking aspen (*Populus tremuloides*), balsam poplar (*Populus balsamifera*) and white spruce (*Picea glauca*). Permafrost has been mapped as continuous (> 90% of the area) north of the Yukon River and discontinuous (50–90%) south of the river (Williams, 1962; Jorgenson *et al*., 2008). Mean daily maximum and minimum temperatures at Fort Yukon (1899 to 1990) are −1°C and −12.6°C, respectively (these data from the National Climate Data Center available at http://www.ncdc.noaa.gov/cdo-web/). Mean annual snowfall for this region is 1.06 m while monthly snowfall ranges from no snow in July and August to 0.17 m in October (these data from the Fish and Wildlife Service are available at http://alaska.fws.gov/nwr/yukonflats/weather.htm).

METHODS

Field Data

Field measurements of ALT were collected during mid-August to early September in 2009 and 2010. Data from both years were combined because there had only been a documented yearly average increase in ALT of 10 cm (~ 11% of the total ALT) and 6 cm (~ 8% of the total ALT) at the Fort Yukon and Circle CALM sites, respectively. Coinciding measurements were made at additional locations to examine the variation in ALT over this time period (Figure 1). Observed values of four sites, located near Canvasback Lake on the Yukon Flats, indicated an average increase in ALT of approximately 3 cm, representing 4 per cent of the total ALT.

We collected one set of observations (n = 137) using a 122-cm long probe to quantify ALT (n = 5/site) within each predefined homogenous transect site (2 m × 14 m). This probing method was appropriate because mineral soil

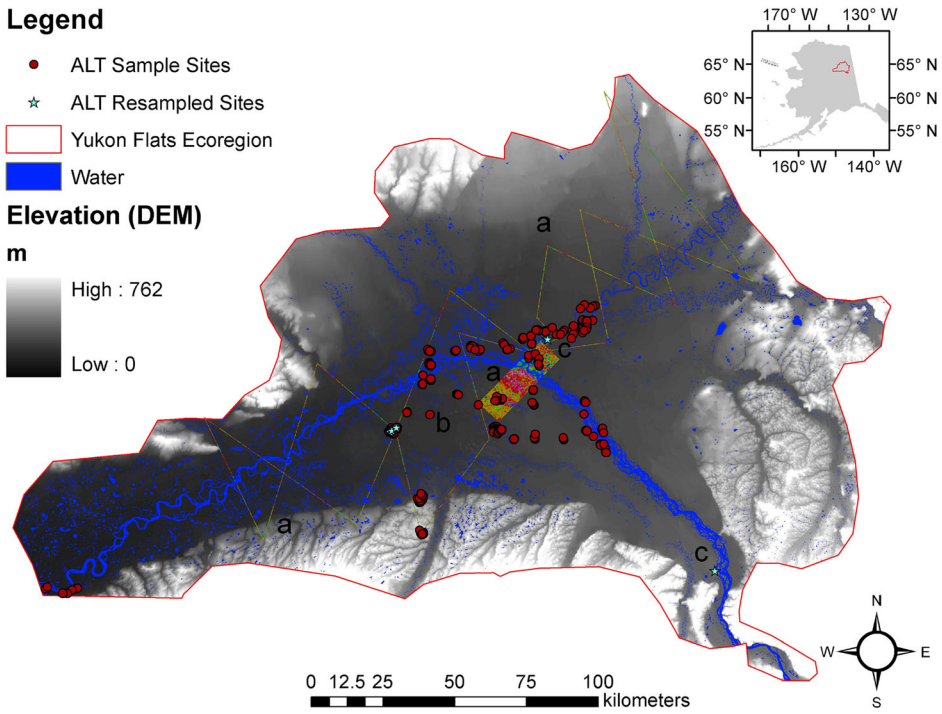

Figure 1 The Yukon Flats Ecoregion overlaid with the 2001 National Land Cover Dataset (water), averaged inverted airborne electromagnetic (AEM) flight line-gridded resistivity (0–2.6 m), active-layer thickness (ALT) sample sites (n = 369), re-sampled alt sites (n = 6) and a re-sampled 30-m digital elevation model (DEM). The elevation is relative to the outlet point of the Yukon River from the ecoregion (in the southwest corner of the image). The AEM survey was conducted in a contiguous block area and along widely spaced reconnaissance lines.

textures were predominately fine-grained. However, if probe refusal was met because rock was encountered instead of permafrost, it was designated accordingly. Multiple measurements within each transect were conducted in order to represent a single Landsat pixel. Subsequently, ALT measurements within each transect were averaged to provide an estimate of the overall transect ALT. Transects in which the observation of the presence/absence of permafrost differed were designated to the majority class, within the appropriate database. ALT measurements were sampled from relatively homogenous plots and represented a range of conditions present within the YFE, which allows for the development of unbiased and equally weighted models.

A second set of observations (n = 232) was developed primarily from point data collected by the Natural Resources Conservation Service soil survey programme, which used a 200-cm long hand soil auger and soil pits to quantify ALT during 2009 and 2010. All field observations were combined into two spatial databases to: (1) estimate ALT < 101 cm; and (2) predict the presence and absence of near-surface permafrost and the associated probability of permafrost occurrence, where 122 cm served as the threshold value for the presence/absence. A value of 101 cm was given to ALT measurements greater than 101 cm and a value of 0 (i.e. unfrozen to a depth of 122 cm) was given to ALT measurements greater than 122 cm for the two distinct spatial databases, respectively. By constraining ALT to this depth, we were able to utilize more field observations. For example, if gravel or compacted sand impeded probe investigations below the 122 cm mark, the measurements would need be discarded because we couldn't guarantee the absence of permafrost within the first 122 cm. The different databases were used for the ALT and permafrost modelling, in order to: (1) establish two end members for depths of observation that were most appropriate for their distinct purposes of modelling and mapping ALT and the presence/absence of permafrost; (2) quantify uncertainty when comparing models and maps; and (3) assess the overall utility of two separate modelling techniques and maps. Field observations used within each database represent the same location, but different subsurface properties (i.e. ALT vs the presence/absence of permafrost). These observations (Figure 1) served as dependent variables within the regression tree and decision tree models.

AEM Survey

The AEM survey was flown in June 2010 over a portion of the YFE (Figure 1), with measurements taken along both widely spaced reconnaissance lines and a contiguous block area (~ 300 km^2) with 350-m line spacing near Fort Yukon. This survey was acquired with the Fugro Resolve (Mississauga, Ontario Canada) frequency domain electromagnetic system (Siemon, 2006), which has six transmitter-receiver coil pairs that operate between 0.4 and 140 kHz (see Ball *et al.*, 2011, for details). Data were acquired from ~ 30 m above the ground surface, at a ground speed of 80–100 km/h and a sampling

rate of 10 Hz. This generated approximately one data point every 3 m along the flight line. AEM data were inverted using a one-dimensional algorithm that solves for the distribution of resistivity as a function of depth given the measured data and system elevation, treating each data location independently (Farquharson *et al*., 2003).

For our analysis, results of the AEM inversions presented by Minsley *et al*. (2012) were interpolated to a 30 x 30-m grid to coincide with the horizontal resolution of our other datasets (e.g. Landsat imagery). This resulted in a number of interpolated cells between flight lines that were less constrained by the data because they were farther from the flight lines. To reduce error, only resistivity values obtained within 30 m of the flight lines were used during model development. While the primary focus of the AEM survey was to image broad lithologic and permafrost features at depths up to 100 m, this study used only NSR values reflective of 0 to 2.6-m depths. Although vertical resolution of NSR is limited because of the physical characteristics of the AEM system, Jepsen *et al*. (2012) found a relationship between shallow resistivity values and the presence or absence of permafrost indicated by frost probes, thus providing support for the utility of shallow AEM resistivity for near-surface permafrost characterisation.

Remote Sensing and Map Data Compilation

A diverse set of dependent variables and independent variables were selected for model development because of their expected relations with permafrost and ALT (Table 1). Specifically, surface vegetation features, captured by remote sensing (i.e. Landsat imagery, spectral indices, biomass), were used to help estimate NSR and ALT because of their likely associations with permafrost. Surficial deposit information was included because lithology and water affect soil thermal properties and NSR. As both vegetation and ALT are impacted by wildfire, it was important to highlight areas of disturbance (e.g. fire perimeters) within the ecoregion. Digital elevation model and derivatives affect permafrost

Table 1 Model input variables and descriptions.

Variable	Description
NDII*	Normalised difference infrared index
Band 5	Landsat TM band 5 at-sensor reflectance
NDII7*	Normalised difference infrared index
NDWI*	Normalised difference water index
Band 4	Landsat TM band 4 at-sensor reflectance
NDVI*	Normalised difference vegetation index
NDWI7*	Normalised difference water index
Band 7	Landsat TM band 7 at-sensor reflectance
GNDVI*	Green normalised difference vegetation index
Band 3	Landsat TM band 3 at-sensor reflectance
Biomass	30-m resolution above-ground biomass dataset (Ji *et al*., 2012)
SAVI*	Soil-adjusted vegetation index
EVI*	Enhanced vegetation index
LST	Land surface temperature
DEM	A USGS digital elevation model that was re-sampled to 30 m from 60 m using bilinear interpolation
Per cent slope	Percentage slope as derived from DEM
Band 2	Landsat TM band 2 at-sensor reflectance
Spatial texture	The averaged coefficient of variation (3 x 3 pixel-moving window), as derived from Landsat imagery (bands 3, 4 and 5)
CTI	Steady-state wetness index that is correlated with several soil attributes: horizon depth, silt percentage, organic matter content (Moore *et al*., 1993). This was re-sampled from 60 m to 30 m using bilinear interpolation
Heat load	Reflects heat load differences where southwest-facing slopes (225° clockwise from north) are the highest and northeast-facing slopes (45°) are the lowest (McCune and Keon, 2002)
Potential incident radiation	Reflects potential incident radiation differences where south-facing slopes are the highest and north-facing slopes are the lowest (i.e. 180° - |Aspect - 180°|) (McCune and Keon, 2002)
Land cover and fire data	See Land Cover and Fire Data section
Surficial geology	General surficial geology (Williams, 1962) which was scanned, georectified and manually digitised. Some boundaries, particularly floodplains, were revised to better align with Landsat images
Field data	See Field Data section for active-layer measurements
AEM survey	See AEM Survey section
Extrapolated resistivity (0–2.6 m)	Estimated near-surface electrical resistivity (ohm-m) (r = 0.86)

*Source: Ji *et al*. (2012, Table 4). See text for other abbreviations.

distribution not only by elevation, incident radiation, slope and aspect, but also by proxies of potential run-on moisture (i.e. compound topographic index, CTI; Moore et al., 1993). Some effort was made during ALT model development to limit the number of input variables while maintaining prediction accuracy. For example, surficial deposits were not used during ALT modelling because of the coarse resolution of the dataset, which resulted in ALT maps containing artefacts and a lack of improvement in model accuracies. However, surficial deposits were used within the resistivity portion of this study, as electrical resistivity was primarily controlled by lithology and the dependent variable (i.e. NSR) dataset was large and spatially exhaustive. These datasets are described in more detail below.

Land Cover and Fire Data.

Land cover data were obtained from the 2001 National Land Cover Dataset produced by the US Geological Survey (USGS) (Homer *et al.*, 2007). Fire perimeter data were obtained through Monitoring Trends in Burn Severity (http://www.mtbs.gov/) for the years 2000 to 2010. Areas containing recent fires, or fires still burning (June 2008 to June 2010), were excluded from the NSR and ALT databases, while fires that occurred from 2000 to April 2008 were given a unique value. This was done because areas of recent fires were more likely to have stand replacement land cover and thicker active layers (Brown, 1983), and there was a need for post-fire spectral values to better spatially coincide with those depicted by Landsat imagery.

Landsat TM Data.

A Landsat TM image mosaic of the YFE at 30-m resolution was developed from six Landsat scenes taken from late August 2008 through early September 2008 (Ji *et al.*, 2012). Level 1 T digital numbers (DN) data of the reflective bands (bands 1 to 5 and 7) for each image were converted to at-sensor radiances and then at-sensor reflectance (Chander and Markham, 2003). The inverse Plank function was used to convert land surface temperature into Kelvin degrees after the DN data of band 6 were converted to at-sensor radiance. Spatial texture products were derived from the mosaic using the ERDAS Imagine focal scan function (ERDAS Field Guide, 2008) to calculate the average coefficient of variation in Landsat bands 3, 4 and 5, within a 3×3 pixel window. These products served as continuous independent variables for model development because of their ability to differentiate areas of heterogeneity, and they have proven useful in past permafrost analysis to help delineate vegetation communities and associated canopy covers (Panda *et al.*, 2012). Areas of high heterogeneity appeared to be associated with lake water edges, drained basins, areas of abrupt change and uncommon land cover types (e.g. moss, barren land). The late-summer Landsat TM mosaic was used because minimal seasonal frost is present in late summer, providing a higher degree of temporal consistency with field ALT measurements. The late-summer season allows surface vegetation, moisture and surface temperature conditions, quantified by Landsat, to better represent late-season ALT. However, it is important to note the difference in dates of data acquisition between Landsat imagery in 2008 and field data in 2009 and 2010. We assumed that this difference had little effect on modelling. Further, by using only observations not affected by recent fires from June 2008 to June 2010, major disturbances between these time periods are accounted for, and only minor changes in ALT should occur.

Statistical Spatial Modelling

Piecewise Regression and Decision Tree Techniques.

Piecewise regressions generalised from a regression tree (RuleQuest, 2004) were used to predict and map NSR and ALT values (< 101 cm). Regression tree analyses are useful for identifying and predicting complex hierarchical relationships in multivariate datasets (Michaelsen *et al.*, 2004). This approach optimises prediction by stratification, allowing representation of non-linear relationships, and mapping of carbon fluxes (Wylie *et al.*, 2007) and continuous fields in land cover (Homer *et al.*, 2009).

Decision tree classification (RuleQuest, 2004) was used to predict the presence and absence of permafrost and the associated probability of permafrost occurrence, where 122 cm below the land surface served as a threshold value for presence/absence. A boosting technique was also used to generate and combine multiple classifiers. This technique has been known to reduce misclassification rates by 20–50 per cent (Friedl *et al.*, 1999) and slightly increased the accuracy of the near-surface permafrost decision tree model.

Validation of the models for NSR, ALT and the presence/absence of permafrost was done using tenfold cross-validations. This validation was employed to utilise all measurements available during model development (field plots were limited and represented a small area of the YFE) and to assess model accuracies on unseen data. The tenfold cross-validations took observations from ten random and equally sized groups. For each random group, a model was constructed from observations in the remaining groups and tested on the observations in the validation group. In this way, each observation was used just once as a test observation.

Additional independent tests were conducted for the ALT modelling, but were relatively limited due to data availability. All models were evaluated using an overall mean absolute error (MAE),

$$\mathrm{MAE} = \frac{1}{n}\sum_{i=1}^{n}\left|Y_i - \hat{Y}_i\right|$$

and mean bias error (MBE),

$$\mathrm{MBE} = \frac{1}{n}\sum_{i=1}^{n}\left(Y_i - \hat{Y}_i\right)$$

for final model selection purposes, where Y_i and $\hat{Y}_i$ are observed measurements and predicted measurements, respectively, for sample i.

Relative MAE and MBE (rMAE and rMBE) were also calculated and used to assess the ratio of error magnitude (MAE and MBE) to the average error magnitude that would result in predicting the mean value. A relative error close to 1 indicates that there is little improvement on the mean, and the independent variables have little predictive capacity. Generally, useful models will have smaller relative errors. Figure 2 provides a schematic layout of the input variables and analytical methods.

Resistivity.

Three depth intervals (0–1 m, 1–2.6 m and 0–2.6 m) were selected initially from the AEM survey to serve as the dependent variable in separate regression tree models. The NSR values from these depths were selected as the dependent variable because independent variables were generally related to surface features. Natural logarithms of NSR were defined as the dependent variable within the singular NSR piecewise regression model. The combined depth interval of 0–2.6 m was also included to develop a model and estimates that better correspond with field measurement depths.

The model only used NSR values within 30 m of the survey flight lines and in areas not affected by recent fires or burning fires. These measurements (n = 110 372) represented a wide range of environmental conditions throughout the ecoregion. Although many independent variables (Table 1) were introduced during model development because of their expected relations with permafrost distribution, actual independent variable usage was much lower (Table 2). Such usage is defined as the per cent of the number of times that a variable was used during model development, relative to the total observations in the model development database.

To assess the effects of fire on NSR, measurements not represented by the 2008 spectral information (i.e. areas of 2009–10 disturbance) (n = 1534) were later used to compare NSR predicted by the model with actual NSR from the inverted resistivity images.

ALT and the Presence/Absence of Near-surface Permafrost.

ALT measurements (n = 369) taken during August and September 2009 and 2010 served as the dependent variable within the ALT piecewise regression model. A single regression tree model was generated from ALT measurements, a portion of the independent variables (Table 2) used in the resistivity extrapolation, and the newly generated NSR map to predict and map ALT < 101 cm.

A boosted decision tree model was then used to classify the presence/absence of permafrost, where 122 cm served as the threshold value above which permafrost was absent. This model was developed for a deeper range than that of the singular ALT piecewise regression tree model because we needed to create more distinctive end members for near-surface and deeper permafrost. Also, by using two different depths during model development and different modelling techniques, we were able to assess and compare spatial estimates and model accuracies. We also assessed the accuracy of the ALT model by comparing mean ALTs calculated by land cover class (Table 3) with ALT for various vegetation types reported in other studies.

The overall representativeness of field data was assessed by calculating an absolute difference map of the singular piecewise regression ALT model, based on varying levels of model extrapolation. This method of extrapolation to quantify uncertainty has been used, for example, to help select optimal locations for future carbon flux towers (Gu *et al.*, 2011). Areas of high

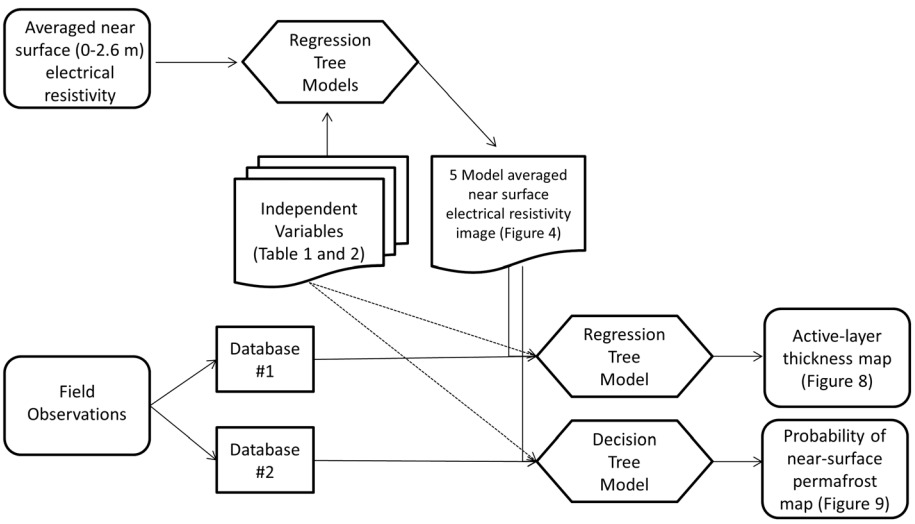

Figure 2 Schematic layout of input variables and analytical methods used within this study.

Table 2 Model input variable usage expressed as a per cent of the total number of times an independent variable was used to predict or stratify, relative to the total number of observations in the model development database: the top five variables used in the model are shown in bold.

	Near-surface resistivity (0–2.6 m)		Active-layer thickness (< 101 cm)		Presence/absence of permafrost (< 122 cm)
Input variable	% Predictors	% Stratifiers	% Predictors	% Stratifiers	% Predictors
NDII	0.90	0.06	0.39		0.43
Band 5	0.91	0.07	0.36		0.56
NDII7	**0.95**	0.08	0.45		**1**
NDWI	0.89	0.1	0.49		**1**
Band 4	0.85	**0.35**	0.37		0.83
NDVI	**0.95**	0.04	**0.54**	0.04	0.36
NDWI7	**0.96**	0.17	0.39	0.07	
Band 7	0.68	**0.46**	0.37	**0.18**	0.82
GNDVI	**0.90**	0.07	**0.51**	0.04	0.47
Band 3	0.90	0.09	0.38		0.88
Biomass	0.86	0.14	**0.56**		0.11
SAVI	**0.93**	0.29	**0.59**		0.13
EVI	0.89	0.02	**0.63**		0.42
LST	0.86	0.06	0.1		0.55
DEM	0.83	**0.88**	0.1	**0.81**	0.89
Per cent slope	0.62		0.42	0.07	0.92
Band 2	0.83	0.25	0.38		0.14
Spatial texture	0.7	0.14	0.03	**0.33**	**1**
CTI	0.53	0.12	0.1	0.17	0.52
Heat load	0.47		0.1		0.78
Potential incident radiation	0.36		0.11	0.01	0.79
Land cover (NLCD) and fire data (MTBS)		**0.73**		**0.28**	**1**
Surficial geology		**0.58**			
Final resistivity (0–2.6 m)-extrapolated map			0.27	**0.24**	**1**

NLCD = National Land Cover Dataset; MTBS = Monitoring Trends in Burn Severity. See Table 1 for other abbreviations.

Table 3 Permafrost probability (within 122 cm) and mean active-layer thickness (ALT) by land cover type.

Land cover in Yukon Flats	Area (km^2)	Field observations (n)	Mean probability of near-surface permafrost (%)	Mean est. ALT (> 101 cm excluded)
Mixed forest	2635	52	85.15	84.86
Sedge/Herbaceous	19	1	82.39	71.16
Evergreen forest	9990	139	66.33	86.64
Woody wetlands	4077	25	64.2	85.77
Deciduous forest	6036	67	45.53	89.41
Shrub/Scrub	2702	6	44.75	76.8
Fires (2001–April 2008)	4419	15	37.89	85.4
Emergent herbaceous wetlands	587	28	28.34	93.47
Grassland/Herbaceous	17	N/A	Masked	Masked
Dwarf shrub	19	N/A	Masked	Masked
Developed	4	N/A	Masked	Masked
Barren land	56	2	Masked	Masked
Open water	2212	34	Masked	Masked

extrapolation are more likely to be associated with uncertainty, as these areas are not represented within model and map development. In order to quantify uncertainty of predicted ALTs, a MAE map was developed. Pixel values of this map represent the MAE of the rule used to predict the estimate.

RESULTS

NSR

A single piecewise regression model developed for mapping NSR in the Yukon Flats, which was based on 23

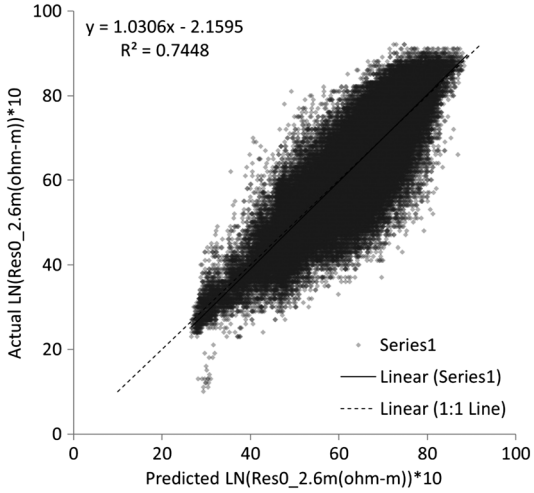

Figure 3 Actual versus predicted (Natural Logarithms (LN) (0−2.6 m) *10) resistivity (ohm-m) values.

independent variables (Table 2), had a high correlation (r = 0.86) between actual and predicted natural logarithms of NSR (Figure 3). A tenfold cross-validation indicated model accuracies were high (r = 0.85) and significant (p 0.001). Error metric calculations, as calculated in linear space, suggest that MBE (174 ohm-m) and MAE (470 ohm-m) were relatively low (rMBE = 0.17; rMAE = 0.44) when compared to the actual mean (1048 ohm-m).

The strongest predictor and stratifier variables used in model development are provided in Table 2. The predictors determined the magnitude of the predicted value, and the stratifiers determined which model was to be used for a given pixel in order to optimise the multiple linear regression prediction. For example,

if: Landsat band 7 > a, land cover = (b, c), and surficial deposit = (d),
then: NSR = c_1 * biomass + c_2 * elevation,

where a is a continuous variable, b, c and d denote categorical variables of land cover and surficial deposit, and c_1 and c_2 are coefficients of the linear model. Very influential variables are highlighted in Table 2 and show strong relationships for several vegetation greenness/productivity indices and for topography, land cover and surficial deposit information. The map of NSR developed from the model is provided in Figure 4.

Mean-estimated NSR varied by nearly tenfold among land cover types and nearly threefold for surficial geology within some land cover types (Figure 5). NSRs were highest for mid- to late-successional forest types and lowest for water, emergent herbaceous wetlands and barrens. Differences among surficial deposits were greater within forested cover types than within shrub and herbaceous cover types, with the exception of dwarf shrub. Within forest cover types, alluvial fan and floodplain deposits, typically underlain by gravel, had mean NSRs that were two to three times

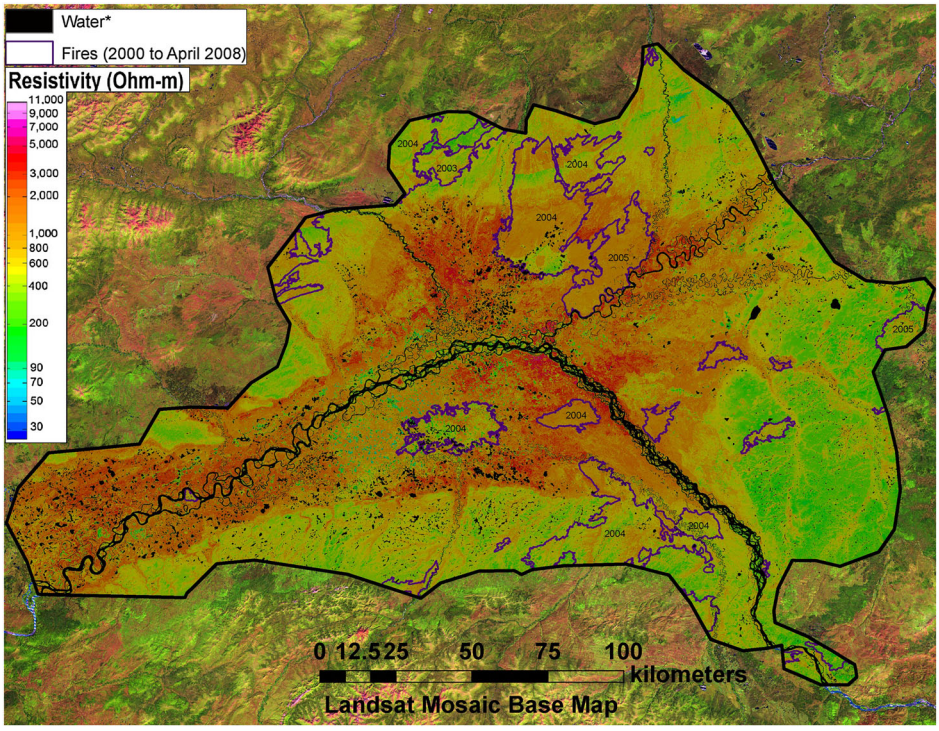

Figure 4 Modelled map of near-surface resistivity (0−2.6 m) surrounded by an Landsat image mosaic. Fires (purple) are from 2000 to April 2008. Water* class is predominantly water, but includes negligible amounts of other masked areas (i.e. grassland/herbaceous, dwarf shrub, barren land, and developed areas)

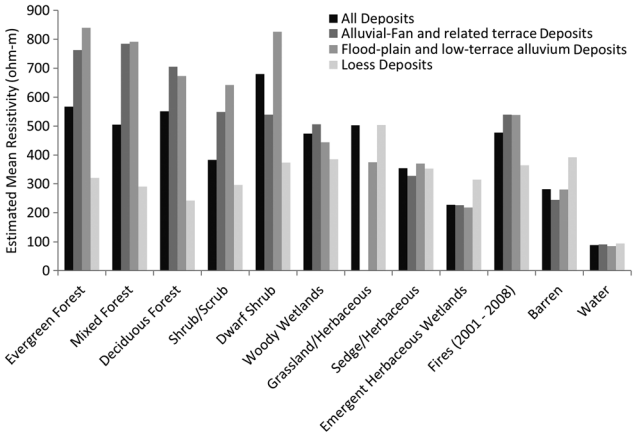

Figure 5 Mean near-surface resistivity by land cover and surficial deposit.

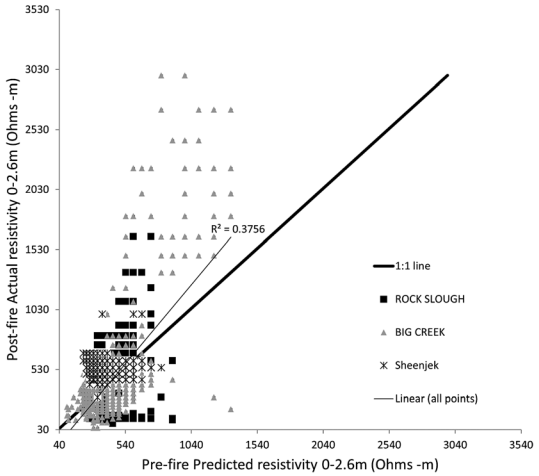

Figure 6 Correlation of near-surface resistivity estimated for pre-fire conditions with measured post-fire inverted resistivity within pre-fire evergreen forest communities.

greater than silty loess deposits. In contrast, for woody, sedge/herbaceous and emergent herbaceous wetlands, which typically have thick surface peat, mean NSRs were similar among surficial deposits.

Recent fires during 2000–08 affected 13 per cent of the area and are likely to have a large effect on ALT and permafrost. A comparison of estimated NSR for pre-fire conditions with actual post-fire inverted resistivity within 30 m of the flight lines showed some divergent trends in NSR among three large fires (Sheenjek, Rock Slough and Big Creek) (Figure 6), which occurred in 2009 and affected 4 per cent of the area. Only evergreen forests were included in this analysis because this restricted changes to a narrow set of environmental conditions where permafrost is nearly always present in pre-fire conditions in this region. While these areas were not implicitly represented within the database, the spatial application of our models allowed us to assess what estimated NSR would have been if these areas had not been affected by fires, based on unburned measurements and relationships elsewhere. Analysis showed that estimated NSR (i.e. pre-fire) and inverted NSR (i.e. post-fire) were significantly correlated ($r = 0.61$, $p < 0.001$) across all fires. Table 4 depicts the assessment of three separate regressions, generated for various fires, where independent data were available across the region. Overall, post-fire inverted NSR tended to be greater (slope = 1.32) than pre-fire estimated NSR, possibly related to the loss of surface organic matter, a temporary increase in soil moisture after the fire, or consequences of estimation algorithms. Error metric calculations show that the MBE (126 ohm-m) is relatively low (rMBE = 0.23) when compared to the actual mean (553 ohm-m). The MAE (183 ohm-m) was higher when compared to the mean (rMAE = 0.40). While estimated NSR was overestimated, the Sheenjek fire displayed an insignificant ($p > 0.05$) and weak correlation ($r = 0.001$) when compared to the post-fire inverted resistivity. Stratified regressions were also developed to assess inter-fire variability and associated error metrics can be seen in Table 4.

ALT and the Presence/Absence of Near-surface Permafrost

ALT (for active layers < 101 cm) was spatially extrapolated across the YFE based on the single piecewise regression model. Highly influential variables in the model included spectral bands, biomass indices, topography, land cover and estimated NSR (Table 2). The Pearson correlation coefficient (r) value for the model was 0.82 ($n = 369$, $p < 0.001$) (Figure 7). ALTs in the map ranged from 25 cm to the maximum 101 cm allowed in the model (Figure 8).

Estimated average results on the validation cases on the piecewise regression tree model had a correlation coefficient value of 0.60 ($n = 1840$, $p < 0.001$). Averaged error metric calculations from the five, tenfold cross-validations show that the bias errors (MBE = −3 cm) and absolute errors

Table 4 Error metric calculations on withheld tests of pre- and post-fire near-surface resistivity (ohm-m).

MTBS fire name	# of test points	Area (km^2)	MAE	rMAE	MBE	rMBE	r	Slope	p
Sheenjek	359	228	159	0.30	135	0.25	0.001	−0.03	> 0.05
Rock Slough	134	282	305	0.54	42	0.07	0.04	0.60	< 0.05
Big Creek	1041	708	175	0.42	−38	−0.09	0.54	1.64	< 0.001

Note: Pearson correlation of coefficient (r), slope and p-value were assessed in linear space, where post-fire resistivity was regressed on pre-fire resistivity. MTBS = Monitoring Trends in Burn Severity. See text for other abbreviations.

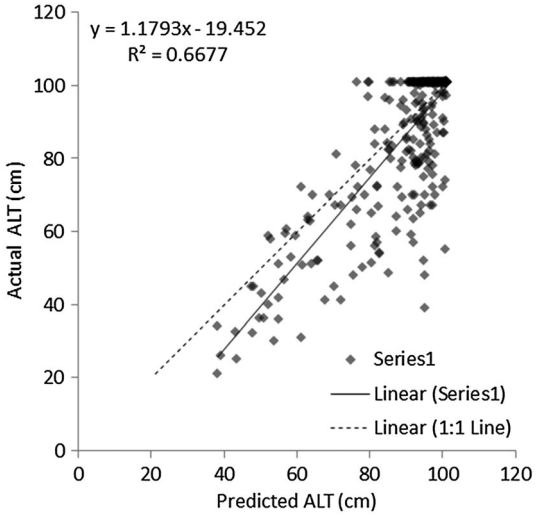

Figure 7 Scatter plot of actual versus predicted active-layer thickness (ALT) of the singular piecewise regression tree model.

(MAE = 11 cm) were relatively low (rMBE = −0.04; rMAE = 0.12) when compared to the actual mean (88 cm). Model estimates tended to overestimate the thickness of the ALT and may be due to truncation of the real ALT > 101 cm to 101 cm.

A boosted decision tree model (accuracy of 87%) was used to classify the presence and absence of near-surface permafrost, where 122 cm below the ground surface served as the threshold value (Figures 9 and 10). When grouped into four classes, permafrost occurrence was highly unlikely (<= 30% probability) on 16 per cent of the YFE, unlikely (> 30 and < 50%) on 20 per cent, likely (> 50 and < 70%) on 22 per cent and highly likely (> = 70%) on 32 per cent of the area. Excluded masked areas (i.e. grassland/herbaceous, dwarf shrub, developed, barren land, open water) and areas of probability equal to 50 per cent covered 7 per cent and 3 per cent of the YFE, respectively. The strongest stratifiers for the presence/absence classification model were spectral indices (i.e. NDII7 and NWDI), spatial texture, land cover updated with fires (2000 to April of 2008) and estimated NSR (Table 2). A series of ten, tenfold cross-validations were then averaged and had an overall accuracy of 72.25 per cent on validation cases.

ALT measurements at two CALM sites (n = 50/site) at Fort Yukon and Circle were also compared to predicted ALT. The CALM sites were established in areas where we had no training data and represent an additional qualitative assessment of model robustness and accuracy. These independent data indicated an overestimation of ALT measurements during the year 2010: actual ALT versus predicted ALT were 93 cm versus 101 cm and 72 cm versus 86 cm at the two sites, respectively.

To evaluate how the model could be improved, we produced an absolute difference map for the singular piecewise regression tree model for ALT to identify areas where model application was extrapolating to new conditions not represented by the model development data (Figure 11a). The results show areas where the ALT model could be improved by gathering additional field data, including recent burns, to better incorporate the effects of fire on permafrost. Note that although the units of the map are in centimetres, this does not actually represent estimation uncertainty. As such, in order to evaluate ALT prediction uncertainty, a MAE map was produced from the rules comprising the singular piecewise regression tree model (Figure 11b). Accordingly, values of this map represent the MAE of the rule used to predict each estimate. Areas represented by high MAE are more likely to be associated with higher prediction errors or discrepancies from the mean. Areas represented by low MAE are more likely to be associated with lower errors or discrepancies from the mean.

DISCUSSION

The modelling approach was able to incorporate point field measurements, NSR measurements from linear AEM surveys, and remotely sensed satellite and map products to produce a regional map of ALT and permafrost occurrence at 30-m resolution. The quantitative modelling approach is similar to the traditional photo-interpreted approach in that it relies on information on topography, surficial deposits, hydrology, vegetation and spectral characteristics, yet has the advantages of providing quantitative estimates of permafrost probability, modelling uncertainty and identifying data gaps where models could be improved. Another strength of this spatial modelling is that input variables can be easily updated with more current imagery, whereas older manual mapping techniques provide static representations, especially for areas with frequent fires.

Influential environmental variables used within the various regression and decision tree models (Table 2) show a strong dependence on surficial deposit information, topography (e.g. slope, elevation), spectral data and indices, spatial texture, land cover and estimated NSR. Influential predictors were more commonly spectral data and indices, while influential stratifiers were elevation, land cover and surficial geology. Heavily utilised spectral indices were related to greenness (i.e. vegetation productivity/stress, moisture, absorbed radiation) and soils (i.e. soil brightness). Such predictors and stratifiers are to be expected, as these variables can help delineate different land characteristics. However, the physical driver behind each predictor variable and subsurface characteristic is harder to assess, as models had complicated interactions. The interaction among the drivers, and their association with physical processes controlling permafrost development, could be assessed by producing more simplistic rule-based models, but likely at the expense of model accuracy. While a diverse set of variables was found to be useful, some variables introduced artefacts within modelled maps. For example, the CTI was useful for modelling ALT, but introduced polygonal shapes into the modelled ALT map within the relatively low-lying alluvial deposits.

At the site scale, the predicted ALTs in this study were similar to those previously observed for different vegetation types (Jorgenson *et al*., 2001b). At Fort Greely in central

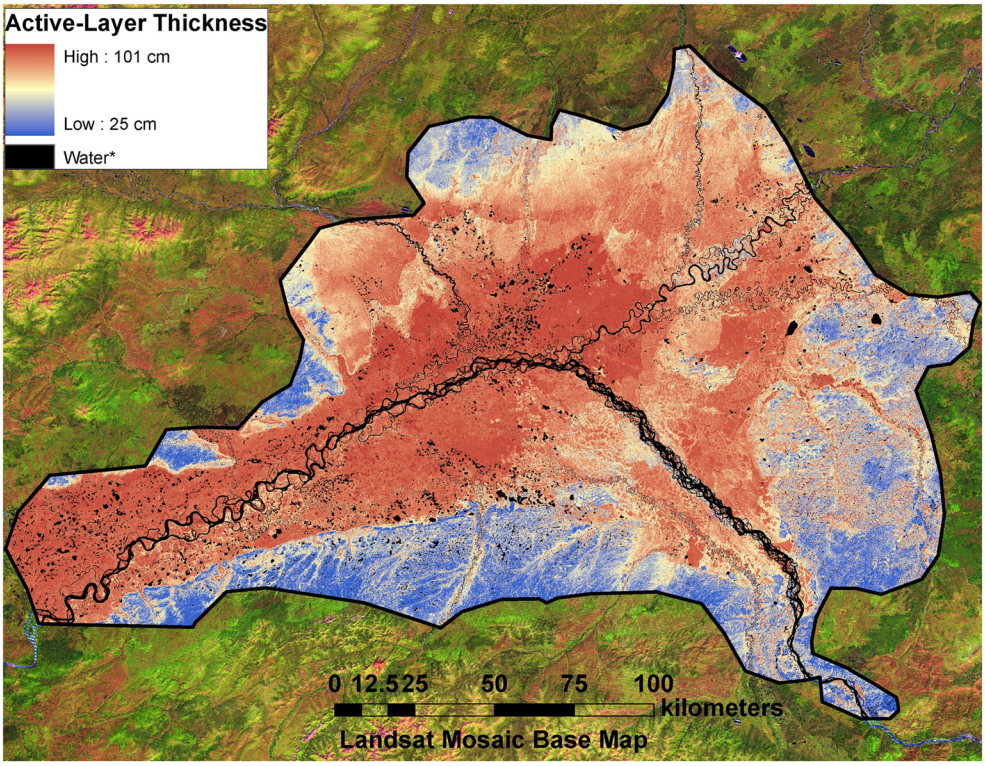

Figure 8 Estimated active-layer thickness (ALT) (< 101 cm) in the Yukon Flats based on a singular piecewise regression tree ALT model. Water class is predominantly water, but includes negligible amounts of other masked areas (i.e. grassland/herbaceous, dwarf shrub, barren land and developed areas).

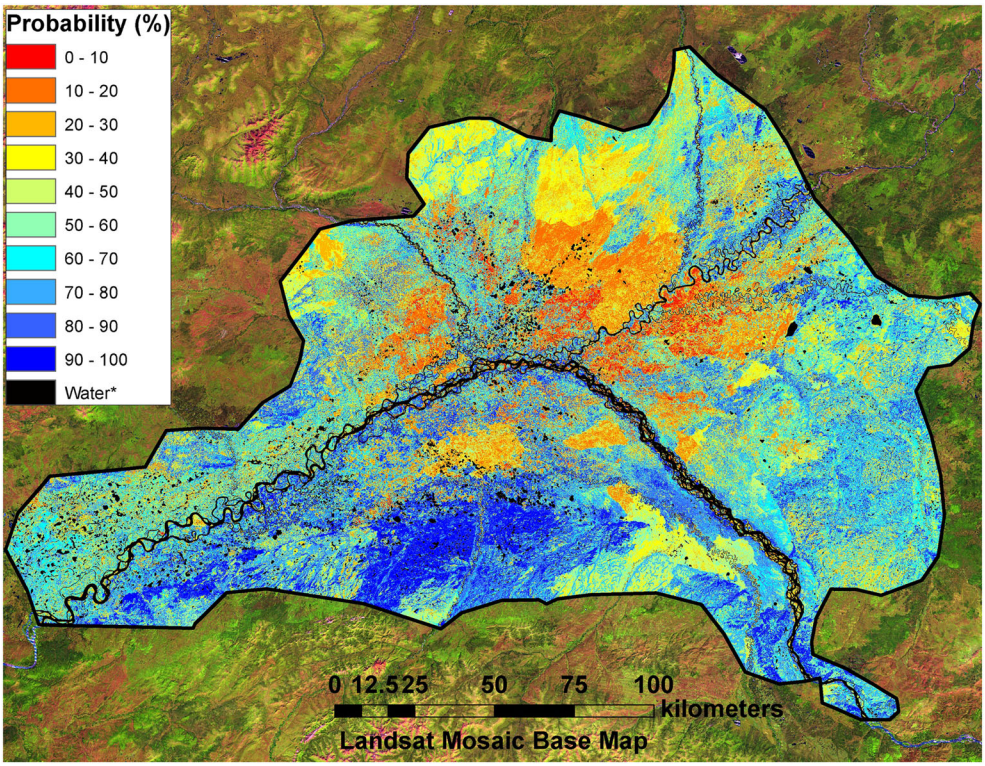

Figure 9 Probability of near-surface permafrost occurrence (within 122 cm) in the Yukon Flats based on a singular decision tree classification model. Water class is predominantly water, but includes negligible amounts of other masked areas (i.e. grassland/herbaceous, dwarf shrub, barren land, and developed areas).

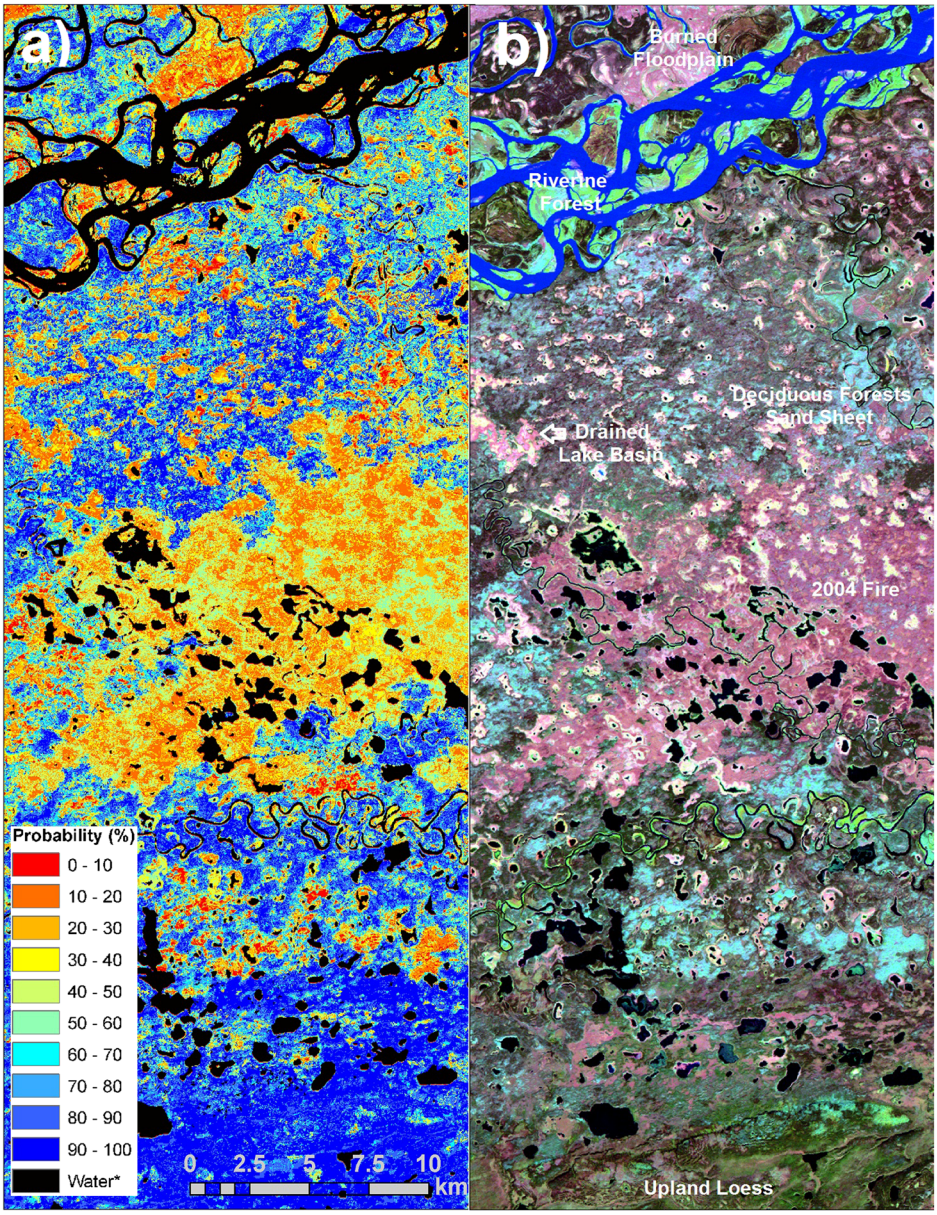

Figure 10 Comparison of (a) permafrost probablity map with (b) Landsat mosaic for an enlarged area that extends from the Yukon River to the loess foothills. Several landscape features are identified on the Landsat mosaic to illustrate predicted permafrost responses to terrain conditions. Water class is predominantly water, but includes negligible amounts of other masked areas (i.e. grassland/herbaceous, dwarf shrub, barren land, and developed areas).

Alaska (Jorgenson *et al*., 2001b), mean ALTs were 70 cm for lowland wet needleleaf forest (black spruce) versus 66 cm for evergreen forest in this study, 118 cm for lowland wet broadleaf forest (paper birch) versus 89 cm for deciduous forest, 106 cm for lowland fen meadow (wet sedge herbaceous) versus 93 cm for emergent herbaceous wetlands and 49 cm for lowland wet tussock scrub versus 71 cm for sedge/herbaceous. The comparison between estimated ALT from the map also corresponded well with ALT measured at two CALM grids.

At the landscape level, estimated ALT was predominately thinner within the higher-elevation loess deposits (i.e. blue area in Figure 8) than the low-lying alluvial and sand sheet deposits (i.e. red area in Figure 8) of the Yukon Flats. On average, low-lying flat areas (slopes 6.15%) within the Yukon Flats were more likely to have permafrost than areas with steeper slopes (79% vs 50%). Similarly, for terrain in the Tanana Valley, permafrost was common in lowlands, on north-facing slopes and in alpine areas (Jorgenson *et al*., 2001b). These landscape differences in ALT are likely due to the strong effects of soil texture on thermal properties and permafrost formation (Jorgenson *et al*., 2001b), which in turn relates to differences in depositional processes (Kreig, 1977). In the

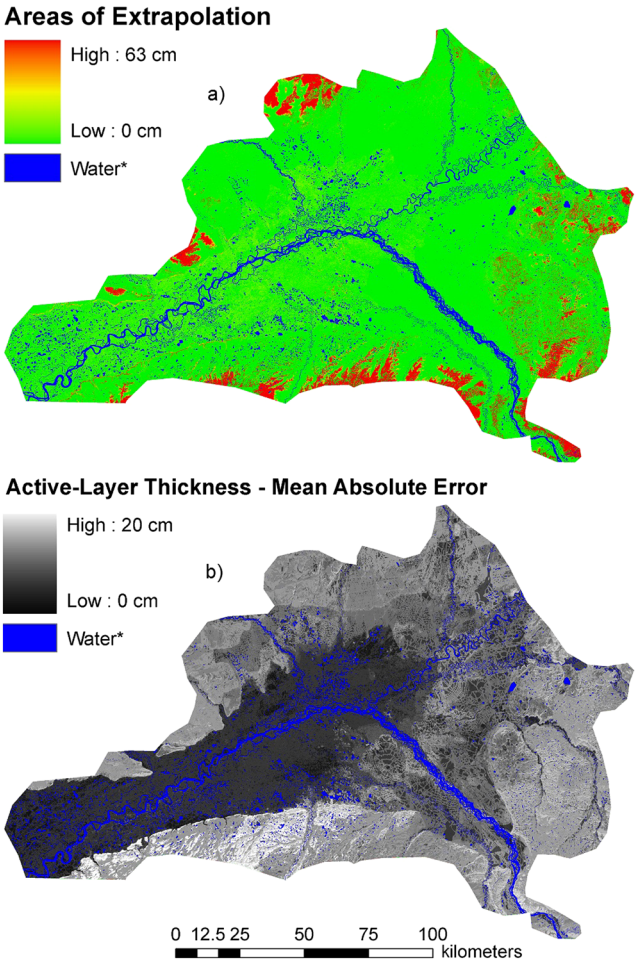

Figure 11 (a) Absolute difference map for the singular piecewise regression tree model for active-layer thickness (ALT) indicating areas where ALT was extraploted beyond the model conditions. (b) Mean average error map for the singular ALT piecewise regression tree model indicating the mean absolute error of the rules used to generate each pixel. Water class is predominantly water, but includes negligible amounts of other masked areas (i.e. grassland/herbaceous, dwarf shrub, barren land, and developed areas).

YFE, permafrost was much less common on floodplains and alluvial fans, which typically have gravel near the surface, than on loess composed of massive silt. The effects of soil properties on thermal regimes and ALT can be further affected by interactions among vegetation cover, soil moisture and organic matter accumulation. For example, the loess deposits, which typically have high moisture contents and thus high thermal conductivities, are dominated by evergreen forests (42%, often stunted black spruce) and shrub/scrub (17%, often dwarf birch or tussocks), which typically have thick surface organic horizons. Our mapping was consistent with observations by Williams (1962) that suggest loess deposits in the southern and eastern portions of the YFE contain substantial amounts of ground ice. Estimating permafrost occurrence in alluvial fans, however, is more problematic because of the high resistivity of gravel and the potential effects of subsurface water movement. There are extensive alluvial fan deposits on the north side of the Yukon River, as well as where the Yukon River enters the flats, where our mapping predicted a low probability of permafrost occurrence. We had no ground data from these areas and little ability to assess the reliability of the mapping.

Fires can have large effects on permafrost stability (Yoshikawa and Hinzman, 2003). Substantial areas within the low-lying interior of the YFE that were affected by fires (2000 to April 2008) had relatively lower NSR values, implying less or deeper permafrost than the surrounding unburned landscape (Figure 4). But when we examined our predicted NSR with actual NSR values from the AEM survey, we found trends were complicated and varied among fires. For the fire-affected areas (Big Creek fire) occurring primarily on loess, NSR values after fire were greater than the pre-fire predictions for areas with high resistivity (areas associated with gravel laden deposits), but lower than pre-fire predictions for areas with low resistivity. For areas on alluvial fan deposits (Sheenjek and Rock Slough fires), actual NSR values were overall lower and higher than predicted for pre-fire conditions. Many factors could have influenced these results, including fire severity, topography, thickening of the active layer, increased wetness from thawing subsurface ice or reduced evapotranspiration, decreased wetness after draining of the thickened active layer, loss of insulating peat, or artefacts of data processing. Further limiting our ability to model permafrost in burned areas was the lack of field data. While the probability map (Figure 9) shows that permafrost is less likely in the burned areas, mean-estimated ALT in the burned areas was similar to that in unburned forest (Table 3). With our limited data, we are cautious about using NSR to assess how permafrost responds to fire given the numerous factors involved; it would be worthy of a future research effort.

Our analyses revealed several limitations to the spatial extrapolation. First, the ALT extrapolation was based upon various ALT measurement sites and there can be a mismatch in the spatial scale of point measurements, which can be highly variable at the microsite scale, with the 30-m mapping resolution. Second, the map represents the general trend in ALT, which showed fairly strong relationships among spatial data and resistivity values within the flats, but the representation of ALT on a pixel-by-pixel basis throughout the entirety of the region is less accurate because of possible disconnects between the temporal variation in AEM, ALT and Landsat data, and the spatial clustering of study sites/pixel values used within model development. However, a Moran's I (0.09) ($p = 0.77$) test for spatial autocorrelation was conducted on all field data and indicated a random dispersion of ALT measurements. Third, there are errors and uncertainty within each of the individual datasets used within this analysis (i.e. resistivity images, land cover, disturbances, field data). Of particular concern is the surficial geology map we used that had insufficient resolution and accuracy to adequately differentiate subsurface characteristics. Direct

measurement of ALT or permafrost presence in relation to NSR is also limited by the quality of information on below-ground stratigraphy, groundwater levels (Ikeda, 2006) and corresponding resistivity freeze-thaw thresholds for different soil types. Finally, areas affected by groundwater movement may have permafrost characteristics that are not reflected well in surface properties used in the spatial extrapolations. Together these factors present challenges for modelling permafrost distribution, yet these uncertainties can be quantified through the statistical modelling approach.

The maps provide a baseline for future monitoring of this area by presenting a quantitative distribution of ALTs. This information is critical for evaluating the active-layer response and perhaps recovery to wildfire, surface water redistribution and climate perturbations. Areas such as the YFE that contain discontinuous permafrost are of particular interest for mapping and monitoring because these areas have relatively warm permafrost (Osterkamp and Romanovsky, 1999), which is generally more unstable and sensitive to a warming climate than continuous permafrost in more northern areas. The maps can serve as inputs and verification for various hydrological models, allowing for improved understanding of streamflow recession (i.e. Lyon *et al*., 2009; Lyon and Destouni, 2010), baseflow magnitude (Ge *et al*., 2011; Walvoord *et al*., 2012), dissolved carbon export (Striegl *et al*., 2005), subartic lake hydrology (Jepsen *et al*., 2012; Wellman *et al*., 2013) and potential future changes to these elements. The maps may also enhance our understanding of the relationships between ALT and the soil organic layer, and subsequently serve as inputs into carbon cycle models by helping estimate soil organic depth and content. NSR, ALT and permafrost probability maps can also give insight into permafrost-fire relationships and thawing processes, be used for land exchange purposes, allow engineers and planners to efficiently develop new infrastructure . (e.g. pipelines and roads), and help emergency management personal mitigate against permafrost-related landslides, flooding, rockfall and avalanches.

CONCLUSION

We mapped near-surface (0–2.6 m) resistivity, ALT (< 101 cm) and the probability of near-surface permafrost occurrence at 30-m resolution for the YFE using field data, AEM survey data, Landsat imagery, surficial geology and other relevant spatial data. A single piecewise regression model for mapping NSR in the Yukon Flats, which was based on 23 independent variables, explained a high proportion of the variance ($r = 0.86$) between actual and predicted natural logarithms of NSR. A piecewise regression model ($r = 0.82$) and a presence/absence decision tree classification (accuracy of 87%) were then used to estimate ALT (< 101 cm), the probability of permafrost occurrence (up to 122 cm) from field data, modelled NSR and other spatial data. This statistical approach provides a quantitative framework for mapping permafrost and ALT with estimated uncertainty. Modelling could be improved by having more field data, higher-quality surficial geology maps and a tighter temporal correspondence among data inputs. Adequately incorporating groundwater effects remains a difficult challenge, but may be improved through the use of higher-resolution topographical data. The results provide a baseline for future permafrost monitoring, serve as inputs for modelling hydrological and carbon cycles at local to regional scales, and offer insight into the ALT response to fire and thaw processes.

ACKNOWLEDGEMENTS

This study was funded by the USGS Climate Land Use Research and Development Program, with initial funding from the USGS Climate Effects Network Yukon River Basin programme (NJP: G10PC00044; LJ: G08PC91508). We thank all of those who have contributed to this project: Norman Bliss (Arctic Slope Regional Corporation Research and Technology Solutions, ASRC), Mark Waldrop (USGS), Kurtis Nelson (USGS), Jack McFarland (USGS), Birgit Peterson (ASRC), Dana Nossov (University of Alaska Fairbanks, UAF), Mark Winterstein (UAF), Darren Van Sistine (USGS) and Jim Webster (bush pilot). We also thank Alessio Gusmeroli, Julian Murton and two anonymous referees for their thoughtful reviews of this manuscript. Any use of trade, firm, or product names is for descriptive purposes only and does not imply endorsement by the U.S. Government.

REFERENCES

Anderson DM, Crowder WK, Gatto LW, Haugen RK, Marlar TL, Mckim HL, Petrone A. 1973. A ERTS view of Alaska, a regional analysis of earth and water resources based on satellite imagery. *US Army Cold Regions Research and Engineering Laboratory Technical Report* 241, 50 pp.

Ball LB, Smith BD, Minsley BJ, Abraham JD, Voss CI, Astley BN, Deszcz-Pan M, Cannia JC. 2011. Airborne electromagnetic and magnetic geophysical survey data of the Yukon Flats and Fort. Wainwright areas, central Alaska, June 2010 *U.S. Geological Survey Open-File Report*. 2011–1304, 21 pp.

Brown RJE. 1983. Effects of fire on the permafrost ground thermal regime. In *The Role of Fire in Northern Circumpolar Ecosystems*, Wein RW, MacLean DA (eds). John Wiley and Sons: Chichester; 97–110.

Burns LE, Fugro Airborne Surveys Corp., Stevens Exploration Management Corp. 2006. Line, grid, and vector data, and plot files for the airborne geophysical survey of the Alaska Highway corridor, east-central Alaska. Alaska Division of Geological & Geophysical Surveys Geophysical Report 2006–6, 1 DVD.

Chander G, Markham BL. 2003. Revised Landsat-5 TM radiometric calibration procedures and post calibration dynamic Ranges. *IEEE Transactions on Geoscience and Remote Sensing* **41**: 2674–2677.

Daniels JJ, Keller GV, Jacobson JJ. 1976. Computer-assisted interpretation of electromagnetic soundings over a permafrost sections. *Geophysics* **41**(4): 752–765.

Duguay CR, Zhang T, Leverington DW, Romanovsky VE. 2005. Satellite remote sensing of permafrost and seasonally frozen

ground. In *Remote Sensing in Northern Hydrology: Measuring Environmental Change*, Duguay CR, Pietroniro A (eds). Geophysical Monograph 163. American Geophysical Union: 91–118.

ERDAS, 2008. *ERDAS Field Guide*, **II**: 132–133, Norcross, GA: ERDAS, Inc.

Farquharson CG, Oldenburg DW, Routh PS. 2003. Simultaneous 1D inversion of loop-loop electromagnetic data for magnetic susceptibility and electrical conductivity. *Geophysics* **68**(6): 1857–1869.

Ferrians OJ, Jr. 1965. Permafrost map of Alaska. US Geological Survey Miscellaneous Geologic Investigations Map I-445, scale 1:2,500,000, 1 sheet.

Friedl MA, Brodley CE, Strahler AH. 1999. Maximizing land cover classification accuracies produced by decision trees at continental to global scales. *IEEE Transactions on Geoscience and Remote Sensing* **37**(2): 969–977.

Gu Y, Howard D, Wylie B, Zhang L. 2011. Mapping carbon flux uncertainty and selecting optimal locations for future flux towers in the Great Plains. *Landscape Ecology*. DOI: 10.1007/s109890-011-9699-7

Hachem S, Allard M, Duguay C. 2009. Using the MODIS land surface temperature product for mapping permafrost: an application to northern Québec and Labrador, Canada. *Permafrost and Periglacial Processes* **20**: 407–416. DOI: 10.1002/ppp.672

Hoekstra P, Sellmann PV, Delaney A. 1975. Ground and airborne resistivity surveys of permafrost near Fairbanks, Alaska. *Geophysics* **40**(4): 641–656.

Homer CG, Aldridge CL, Meyer DK, Coan MJ, Bowen ZH. 2009. Multiscale sagebrush rangeland habitat modeling in southwest Wyoming. *US Geological Survey Open-File Report* 2008–1027, 14 pp.

Homer C, Dewitz J, Fry J, Coan M, Hossain N, Larson C, Herold N, McKerrow A, VanDriel JN, Wickham J. 2007. Completion of the 2001 National Land Cover Database for the Conterminous United States. *Photogrammetric Engineering and Remote Sensing* **73**(4): pp 335–341.

Ikeda A. 2006. Combination of conventional geophysical methods for sounding the composition of rock glaciers in the Swiss Alps. *Permafrost and Periglacial Processes* **17**: 35–48.

Jepsen SM, Voss CI, Walvoord MA, Rose JR, Smith BD, Minsley BJ. 2012. Sensitivity analysis of lake mass balance in discontinuous permafrost: Example from disappearing Twelvemile Lake, Yukon Flats, Alaska (USA). *Hydrogeology Journal*. DOI: 10.1007/s10040-012-0896-5

Ji L, Wylie BK, Nossov DR, Peterson B, Waldrop MP, McFarland JW, Rover J, Hollingsworth TN. 2012. Estimating aboveground biomass in interior Alaska with Landsat data and field measurements. *International Journal of Applied Earth Observation and Geoinformation*.

Joesting HR. 1941. Magnetometer and direct-current resistivity studies in Alaska. Mineral Industry Research Laboratory, University of Alaska Fairbanks. Reprinted in 1979 as MIRL Special Paper #2, 34 pp.

Jorgenson MT, Roth JE, Smith MD, Schlentner S, Lentz W, Pullman ER. 2001a. An ecological land survey for Fort Greely, Alaska. US Army Cold Regions Research and Engineering Laboratory, Hanover, NH, ERDC/CRREL TR-01-04, 85 pp.

Jorgenson MT, Racine C, Walters J, Osterkamp T. 2001b. Permafrost degradation and ecological changes associated with a warming climate in central Alaska. *Climate Change* **48**(4): 551–579. DOI: 10.1023/A:1005667424292

Jorgenson MT, Shur YL, Pullman ER. 2006. Abrupt increase in permafrost degradation in Arctic Alaska. *Geophysical Research Letters* **33**: L02503. DOI: 10.1029/2005GL024960

Jorgenson T, Yoshikawa K, Kanevskiy M, Shur Y, Romanovsky V, Marchenko S, Grosse G, Brown J, Jones B. 2008. Permafrost characteristics of Alaska – a new permafrost map of Alaska. Paper presented at the Ninth International Conference on Permafrost, University of Alaska Fairbanks, Fairbanks.

Kawaski K, Osterkamp TE. 1989. Mapping shallow permafrost by electromagnetic induction; Practical considerations. *Cold Regions Science and Technology* **15**(3): 279–288.

Kneisel C, Hauck C, Fortier R, Moorman B. 2008. Advances in Geophysical Methods of Permafrost Investigations. *Permafrost and Periglacial Processes* **19**: 157–178. DOI: 10.1002/ppp.616

Kreig RA. 1977. Terrain analysis for the Trans-Alaska pipeline. *Civil Engineering ASCE* **47**(7): 61–65.

Kremer M, Lewkowicz AG, Bonnaventure PP, Sawada MC. 2011. Utility of Classification and Regression Tree Analyses and Vegetation in Mountain Permafrost Models, Yukon, Canada. *Permafrost and Periglacial Processes* **22**(2): 163–178. DOI: 10.1002/ppp.719

Lewkowicz AG, Ednie M. 2004. Probability mapping of mountain permafrost using the BTS method, Wolf Creek, Yukon Territory, Canada. *Permafrost and Periglacial Processes* **15**: 67–80. DOI: 10.1002/ppp.480

Lyon SW, Destouni G. 2010. Changes in catchment-scale recession flow properties in response to permafrost thawing in the Yukon River Basin. *International Journal of Climatology* **30**: 2138–2145. DOI: 10.1002/joc.1993.

Lyon SW, Destouni G, Giesler R, Humborg C, Mörth M, Seibert J, Karlsson J, Troch PA. 2009. Estimation of permafrost thawing rates in a sub-arctic catchment using recession flow analysis. *Hydrology and Earth System Sciences* **13**: 595–604. DOI: 10.5194/hess-13-595-2009

McCune B, Keon D. 2002. Equations for potential annual direct incident radiation and heat load. *Journal of Vegetation Science* **13**: 603–606. DOI: 10.1111/j.1654-1103.2002.tb02087.x

Michaelsen J, Schimel DS, Friedl MA, Davis FW, Dubayah RC. 2004. Regression tree analysis of satellite and terrain data to guide vegetation sampling and surveys. *Journal of Vegetation Science* **5**: 673–686. DOI: 10.2307/3235882

Minsley BJ, Abraham JD, Smith BD, Cannia JC, Voss CI, Jorgenson MT, Walvoord MA, Wylie BK, Anderson L, Ball LB, Deszcz-Pan M, Wellman TP, Ager TA. 2012. Airborne electromagnetic imaging of discontinuous permafrost. *Geophysical Research Letters* **39**: L02503. DOI: 10.1029/2011GL050079

Moore ID, Gessler PE, Nielsen GA, Petersen GA. 1993. Terrain attributes: estimation methods and scale effects. In *Modeling Change in Environmental Systems*, Jakeman AJ, Beck MB, McAleer M (eds). John Wiley & Sons: London; 189–214.

Morrissey LA, Strong L, Card DH. 1986. Mapping permafrost in the boreal forest with Thematic Mapper satellite data. *Photogrammetric Engineering and Remote Sensing* **52**: 1513–1520.

Nowacki G, Spencer P, Brock T, Fleming M, Jorgenson T. 2002. Ecoregions of Alaska and Neighboring Territories. *US Geological Survey Open File Report* 02–297.

Osterkamp TE, Romanovsky VE. 1999. Evidence for warming and thawing of discontinuous permafrost in Alaska. *Permafrost and Periglacial Processes* **10**(1): 17–37. DOI: 10.1002/(SICI)1099-1530

Panda SK, Prakash A, Solie DN, Romanovsky VE, Jorgenson MT. 2010. Remote sensing and field-based mapping of permafrost distribution along the Alaska Highway corridor, Interior Alaska. *Permafrost and Periglacial Processes* **21**: 271–281.

Panda SK, Prakash AM, Jorgenson T, Solie DN. 2012. Near-surface permafrost distribution mapping using logistic regression and remote sensing in Interior Alaska. *GIScience and Remote Sensing* **49**(3): 346–363.

Peddle DR. 1991. Evidential classification of land cover and permafrost from multisource remote sensing imagery in mountainous terrain, YukonUnpublished MSc thesis,

Department of Geography, University of Calgary, Alberta, Canada, 178 pp.

Reger RD, Hubbard TD, Gallagher PE. 2012. Reconnaissance interpretation of 1978–1981 permafrost, Alaska Highway corridor, Tetlin Junction to Canada border, Alaska. Alaska Division of Geological & Geophysical Surveys, Fairbanks, AK. Preliminary Interpretive Report 2012-1C, 27 pp.

Roth K, Bolke J, Vogel H. 2005. Quantifying permafrost patterns using Minkowski densities. *Permafrost and Periglacial Processes* **16**(3): 277–290. DOI: 10.1002/ppp.531

RuleQuest. 2004. An overview of Cubist. http://www.rulequest.com/cubist-unix.html [20 June 2011].

Siemon B. 2006. Electromagnetic methods - frequency domain. In *Groundwater Geophysics: A Tool for Hydrogeology*, Kirsch R (ed). Springer-Verlag: Berlin; 155–176.

Siemon B, Christiansen AV, Auken E. 2009. A review of helicopter-borne electromagnetic methods for groundwater exploration. *Near Surface Geophysics* **7**(5–6): 629–646.

Striegl RG, Aiken GR, Dornblaser MM, Raymond PA, Wickland KP. 2005. A decrease in discharge-normalized DOC export by the Yukon River during summer through autumn. *Geophysical Research Letters* **32**: L21413.

Walvoord MA, Voss CI, Wellman TP. 2012. Influence of permafrost distribution on groundwater flow in the context of climate-driven permafrost thaw: Example from Yukon Flats Basin, Alaska, USA. *Water Resources Research*, **48**, W07524. DOI: 10.1029/2011WR011595

Wellman TP, Voss CI, Walvoord MA. 2013. Impacts of climate, lake size, and supra- and sub-permafrost groundwater flow on lake-talik evolution, Yukon Flats, Alaska, USA. *Hydrogeology Journal*. DOI: 10.1007/s10040-012-0941-4

Williams JR. 1962. Geologic reconnaissance of the Yukon Flats District Alaska. *US Geological Survey Bulletin* **1111-H**: 289–331.

Wylie BK, Fosnight EA, Gilmanov TG, Frank AB, Morgan JA, Haferkamp MR, Meyers TP. 2007. Adaptive data-driven models for estimating carbon fluxes in the northern Great Plains. *Remote Sensing of Environment* **106**(4): 399–413.

Yoshikawa K, Hinzman LD. 2003. Shrinking thermokarst ponds and groundwater dynamics in discontinuous permafrost. *Permafrost and Periglacial Processes* **14**(2): 151–160.